Liquid Crystals
Publication details, including instructions for authors and subscription information:
http://www.informaworld.com/smpp/title~content=t713926090

Computer simulation studies of anisotropic systems. XIX. Mesophases formed by the Gay-Berne model mesogen

G. R. Luckhurst[a]; R. A. Stephens[a]; R. W. Phippen[b]
[a] Department of Chemistry, The University, Southampton, England [b] BM UK Scientific Centre, Winchester, England

To cite this Article Luckhurst, G. R. , Stephens, R. A. and Phippen, R. W.(1990) 'Computer simulation studies of anisotropic systems. XIX. Mesophases formed by the Gay-Berne model mesogen', Liquid Crystals, 8: 4, 451 — 464
To link to this Article: DOI: 10.1080/02678299008047361
URL: http://dx.doi.org/10.1080/02678299008047361

LIQUID CRYSTALS, 1990, VOL. 8, NO. 4, 451–464

Computer simulation studies of anisotropic systems
XIX. Mesophases formed by the Gay–Berne model mesogen†

by G. R. LUCKHURST and R. A. STEPHENS
Department of Chemistry, The University, Southampton SO9 5NH, England
and R. W. PHIPPEN
IBM UK Scientific Centre, Athelstan House, St. Clement Street,
Winchester SO23 9DR, England

(*Received 9 March 1990; accepted 9 May 1990*)

We report the results of a molecular dynamics computer simulation of particles interacting via the Gay–Berne potential with parameters selected to approximate those of mesogenic molecules. The system was found to form a variety of mesophases as the temperature was lowered. We have characterized these phases with the aid of computer graphics techniques to visualize the molecular organization within configurations taken from the production stage of the simulations. The phases have been identified, on the basis of such images, as isotropic, nematic, smectic A, smectic B and crystal.

1. Introduction

The major requirement for a compound to form a liquid crystal mesophase is that its constituent molecules deviate from spherical symmetry. Although molecules with a wide range of shapes have been found to exhibit liquid crystals the most common form is undoutedly rod-like [1]. In consequence the majority of computer simulations of liquid crystal behaviour have taken the particles to be cylindrically symmetric. The pioneering Monte Carlo simulations by Lebwohl and Lasher assumed a weak anisotropic potential [2], analogous to that expected at long range. However it is appreciated that for real mesogens the anisotropic potential has important contributions from repulsive short range as well as the attractive long range interactions. In an attempt to provide computationally simple potentials for relatively complex molecules Berne and his colleagues have developed a series of potentials based on the gaussian overlap model [3]. Although the earlier versions of these were used in computer simulations of liquid crystal behaviour, apparently with some success, it was realized, eventually, that the Berne–Pechukas–Kushick potential had several unrealistic features [4]. Thus for parallel molecules the well depth is independent of their orientation with respect to the intermolecular vector. In addition the width of the attractive well was found to vary with the molecular orientation with respect to the intermolecular vector.

To rectify these deficiencies Gay and Berne have modified the original gaussian overlap potential in an essentially phenomenological manner [5]. Thus, they attempted to obtain a function which gave the best fit to the pair potential for a linear array of

† Presented at the Twelfth International Liquid Crystal Conference, 15–19 August 1988, University of Freiburg, F.R. Germany.

0267-8292/90 $3.00

four equidistant Lennard-Jones centres with a separation of $2\sigma_0$ between the first and fourth sites. The form adopted for the total potential is

$$U(\hat{\mathbf{u}}_1, \hat{\mathbf{u}}_2, \mathbf{r}) = 4\varepsilon(\hat{\mathbf{u}}_1, \hat{\mathbf{u}}_2, \hat{\mathbf{r}}) \times \left[\left\{\frac{\sigma_0}{r - \sigma(\hat{\mathbf{u}}_1, \hat{\mathbf{u}}_2, \hat{\mathbf{r}}) + \sigma_0}\right\}^{12} - \left\{\frac{\sigma_0}{r - \sigma(\hat{\mathbf{u}}_1, \hat{\mathbf{u}}_2, \hat{\mathbf{r}}) + \sigma_0}\right\}^{6}\right], \quad (1)$$

where $\hat{\mathbf{u}}_1$, $\hat{\mathbf{u}}_2$ are unit vectors giving the orientation of the two particles, $\mathbf{r}$ is the intermolecular vector, the associated unit vector is $\hat{\mathbf{r}}$ and r is the molecular separation. The parameters in the potential are orientation dependent; $\varepsilon(\hat{\mathbf{u}}_1, \hat{\mathbf{u}}_2, \hat{\mathbf{r}})$ is the well depth and $\sigma(\hat{\mathbf{u}}_1, \hat{\mathbf{u}}_2, \hat{\mathbf{r}})$ is the intermolecular separation at which the attractive and repulsive terms cancel. The functional dependence of this distance is, as in the Berne–Pechukas–Kushick potential,

$$\sigma(\hat{\mathbf{u}}_1, \hat{\mathbf{u}}_2, \mathbf{r}) = \sigma_0\left[1 - \tfrac{1}{2}\chi\left\{\frac{(\hat{\mathbf{r}}\cdot\hat{\mathbf{u}}_1 + \hat{\mathbf{r}}\cdot\hat{\mathbf{u}}_2)^2}{1 + \chi(\hat{\mathbf{u}}_1\cdot\hat{\mathbf{u}}_2)} + \frac{(\hat{\mathbf{r}}\cdot\hat{\mathbf{u}}_1 - \hat{\mathbf{r}}\cdot\hat{\mathbf{u}}_2)^2}{1 - \chi(\hat{\mathbf{u}}_1\cdot\hat{\mathbf{u}}_2)}\right\}\right]^{-1/2}, \quad (2)$$

where σ_0 is a constant which we shall identify shortly. The shape anisotropy parameter, χ, is

$$\chi = \{(\sigma_e/\sigma_s)^2 - 1\}/\{(\sigma_e/\sigma_s)^2 + 1\}, \quad (3)$$

where σ_e is the separation when the molecules are end-to-end and σ_s that when they are side-by-side. In other words σ_e and σ_s are essentially the length and breadth of the particle; χ vanishes for spherical particles and is one for infinitely long rods and minus one for infinitely thin disks.

We shall write the depth of the well as

$$\varepsilon(\hat{\mathbf{u}}_1, \hat{\mathbf{u}}_2, \hat{\mathbf{r}}) = \varepsilon_0\varepsilon^{\nu}(\hat{\mathbf{u}}_1, \hat{\mathbf{u}}_2)\varepsilon'^{\mu}(\hat{\mathbf{u}}_1, \hat{\mathbf{u}}_2, \hat{\mathbf{r}}), \quad (4)$$

where

$$\varepsilon_0\varepsilon(\hat{\mathbf{u}}_1, \hat{\mathbf{u}}_2) = \varepsilon_0\{1 - \chi^2(\hat{\mathbf{u}}_1\cdot\hat{\mathbf{u}}_2)^2\}^{-1/2}, \quad (5)$$

as in the original Berne–Pechukas–Kushick potential [3]. The new term has an angular dependence reminiscent of that for $\sigma(\hat{\mathbf{u}}_1\,\hat{\mathbf{u}}_2, \hat{\mathbf{r}})$ namely

$$\varepsilon'(\hat{\mathbf{u}}_1, \hat{\mathbf{u}}_2, \hat{\mathbf{r}}) = 1 - (\chi'/2)\left\{\frac{(\hat{\mathbf{r}}\cdot\hat{\mathbf{u}}_1 + \hat{\mathbf{r}}\cdot\hat{\mathbf{u}}_2)^2}{1 + \chi'(\hat{\mathbf{u}}_1\cdot\hat{\mathbf{u}}_2)} + \frac{(\hat{\mathbf{r}}\cdot\hat{\mathbf{u}}_1 - \hat{\mathbf{r}}\cdot\hat{\mathbf{u}}_2)^2}{1 - \chi'(\hat{\mathbf{u}}_1\cdot\hat{\mathbf{u}}_2)}\right\}, \quad (6)$$

where the parameter χ' is related to the anisotropy in the well depth via

$$\chi' = \{1 - (\varepsilon_e/\varepsilon_s)^{1/\mu}\}/\{1 + (\varepsilon_e/\varepsilon_s)^{1/\mu}\}. \quad (7)$$

The well depth $\varepsilon(\hat{\mathbf{u}}_1, \hat{\mathbf{u}}_2, \hat{\mathbf{r}})$ and the intermolecular separation $\sigma(\hat{\mathbf{u}}_1, \hat{\mathbf{u}}_2, \hat{\mathbf{r}})$ clearly change with the orientations of the molecules and the intermolecular vector. To illustrate this dependence as well as the significance of the parameters σ_e, σ_s, ε_e and ε_s we give in the table the values of $\varepsilon(\hat{\mathbf{u}}_1, \hat{\mathbf{u}}_2, \hat{\mathbf{r}})$ and $\sigma(\hat{\mathbf{u}}_1, \hat{\mathbf{u}}_2, \hat{\mathbf{r}})$ for orientations of particular significance and simplicity. These are the end-to-end (e), the side-by-side (s), the cross (X) and the tee (T) configurations. From the table we can see that in the cross configuration both the well depth and the intermolecular separation are independent of the parameters χ, χ', ν and μ characterizing the Gay–Berne potential; they are just ε_0 and σ_0, respectively. When the molecules are in the side-by-side configuration the intermolecular separation is also σ_0 and so it seems logical to

The well depth $\varepsilon(\hat{\mathbf{u}}_1, \hat{\mathbf{u}}_2, \hat{\mathbf{r}})$ and intermolecular separation $\sigma(\hat{\mathbf{u}}_1, \hat{\mathbf{u}}_2, \hat{\mathbf{r}})$ for particular orientational configurations.

Configuration	$\sigma(\hat{\mathbf{u}}_1, \hat{\mathbf{u}}_2, \hat{\mathbf{r}})$	$\varepsilon(\hat{\mathbf{u}}_1, \hat{\mathbf{u}}_2, \hat{\mathbf{r}})$
e	$\sigma_0\sigma_e/\sigma_s \quad (\equiv \sigma_e)$	$\varepsilon_0(\varepsilon_e/\varepsilon_s)(1 - \chi^2)^{-\nu/2}$
s	$\sigma_0 \quad (\equiv \sigma_s)$	$\varepsilon_0(1 - \chi^2)^{-\nu/2}$
X	$\sigma_0 \quad (\equiv \sigma_s)$	ε_0
T	$\sigma_0\sqrt{\{(\sigma_e/\sigma_s)^2 + 1\}/2}$	$\varepsilon_0\{2/[(\varepsilon_s/\varepsilon_e)^{1/\mu} + 1]\}^{\mu}$

identify this as σ_s. With this identification the separation in the end-to-end configuration is σ_e as we might have anticipated. The well depths for these two configurations do not have such a simple interpretation for they both depend on the shape anisotropy parameter χ and are not simply ε_e and ε_s. However the ratio of the well depths for the end-to-end and side-by-side configurations is just $\varepsilon_e/\varepsilon_s$. In the tee configuration neither the well depth nor the intermolecular separation takes a particularly simple form. The exponents ν and μ in equation (4) are treated as adjustable parameters; to obtain the best fit to the linear array of four Lennard-Jones centres ν was set equal to 1 and μ was equal to 2.

The ability of particles interacting via this particular form of the Gay–Berne potential to exhibit liquid-crystalline behaviour has been studied using the molecular dynamics computer simulation technique [6]. The length-to-breadth ratio, σ_e/σ_s, was set equal to 3 which is typical of a mesogenic molecule and $\varepsilon_e/\varepsilon_s$ was given the value of 1/5 found for the linear array of four Lennard-Jones centres [5]. It was discovered that at a scaled density ρ^* $(\equiv N\sigma_0^3/V)$ of 0·32 and for scaled temperatures T^* $(\equiv kT/\varepsilon_0)$ less than 1·7 the system exhibits a nematic phase with long range orientational order and just short range translational order. In this simulation we had not attempted to locate other liquid crystal phases such as a smectic A which has a layer structure with short range translational order within the layers [7]. However, in computer simulations of hard spherocylinders with a length-to-breadth ratio of 6 : 1 Frenkel has discovered that this system can exist, not only as a nematic phase, but also as a smectic A phase at a higher density [8]. In contrast it has been argued by Frenkel that it is most unlikely that a smectic phase could be formed by hard ellipsoids [9]. It is important therefore in judging the likely phase behaviour of a set of particles interacting via the Gay–Berne or indeed any potential model to know their shape. This may be defined in a variety of ways and for our purposes here we take the shape to given by the contour corresponding to the change of the potential energy from positive to negative. Since we wish to visualize this contour in two dimensions we must also constrain the molecular orientations and we take the particles to be parallel so that the remaining variable is their orientation to the intermolecular vector. This contour is obtained directly from $\sigma(\hat{\mathbf{u}}_1, \hat{\mathbf{u}}_2, \hat{\mathbf{r}})$ given by equation (2) and is shown in figure 1 together with several other contours for different values of the attractive potential energy. These were calculated with the choice of parameters used in the computer simulation experiments and described in the following section. We see from such contours that the shape of the particles interacting via the Gay–Berne intermolecular potential is ellipsoidal and certainly not spherocylindrical. In consequence we might be led to expect that the search for a smectic phase formed by such particles would be fruitless. However the strong side-by-side interactions ($\varepsilon_s > \varepsilon_e$) for this

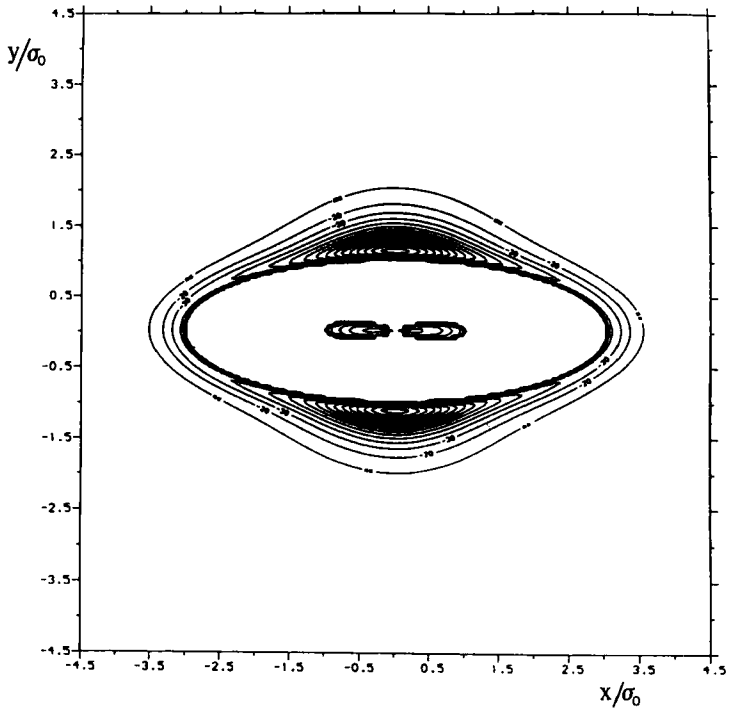

Figure 1. Potential energy contours calculated for parallel molecules interacting via the Gay–Berne potential as a function of their separation and their orientation with respect to the intermolecular vector. The parameterisation of the potential is that used in the molecular dynamics simulation and described in the text.

potential model should stabilize the smectic phase even though the shape of the particle is ellipsoidal. This turns out to be the case and here we describe the results of our simulation experiments.

2. Molecular dynamics simulation

The parameterization of the well depth function $\varepsilon(\hat{\mathbf{u}}_1, \hat{\mathbf{u}}_2, \hat{\mathbf{r}})$ used in the simulation differed slightly from that employed previously. Thus the exponents $\nu = 2$ and $\mu = 1$ were used rather than $\nu = 1$ and $\mu = 2$; this does not influence the relative well depths for the side-by-side or end-to-end configurations. However with the new parameterization the side-by-side configuration is relatively more stable with respect to the cross and tee configurations. Since these configurations are not compatible with the molecular organization within a liquid crystal phase we expect this new parameterization of the Gay–Berne potential to have a greater propensity for mesophase formation. The variation of the scaled potential energy $U(\hat{\mathbf{u}}_1, \hat{\mathbf{u}}_2, \hat{\mathbf{r}})/\varepsilon_0$ as a function of the scaled molecular separation, r/σ_0, for these particular configurations calculated for the two choices of exponents are shown in figure 2.

The system studied contained 256 particles with the usual cubic periodic boundary conditions, nearest image summation and a cut-off of $3{\cdot}8\sigma_0$. The ratios σ_e/σ_s and $\varepsilon_e/\varepsilon_s$ were assigned the values used in the previous simulation [6]. Similarly, the scaled component of the inertia tensor perpendicular to the molecular symmetry axis ($I_\perp^* = I_\perp/m\sigma_0^2$) was assigned the value of 4. This was chosen to ensure that the

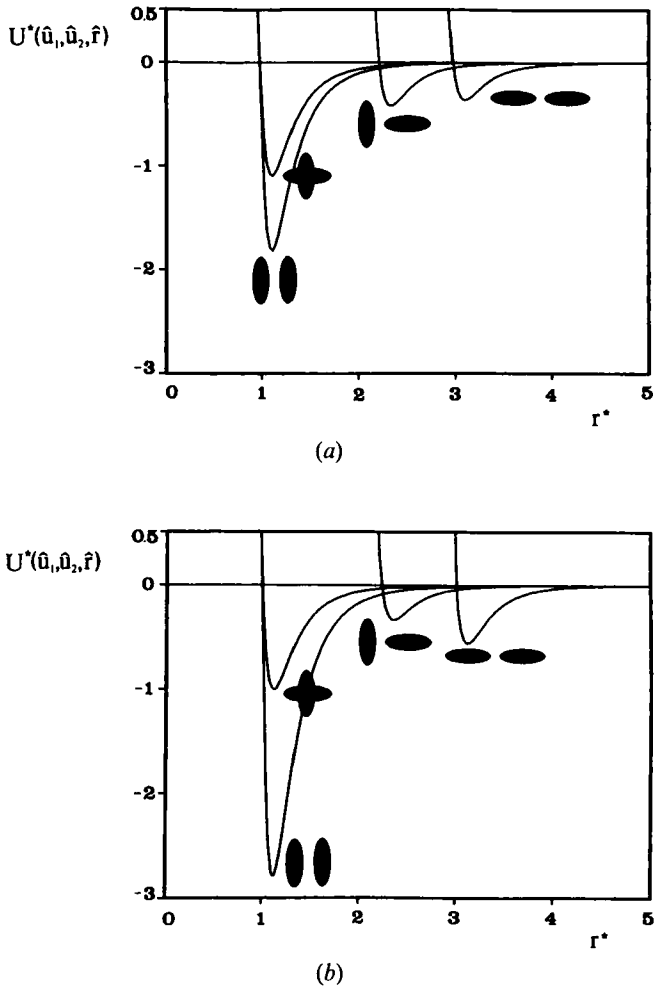

Figure 2. The distance dependence of the energy calculated from the Gay–Berne potential for particular orientations of the molecules with respect to each other and to the intermolecular vector. The exponents were assigned (*a*) their original values, $\nu = 1$ $\mu = 2$, and (*b*) the values $\nu = 2$, $\mu = 1$ employed in this investigation. The ratios of the other parameters, σ_e/σ_s and $\varepsilon_e/\varepsilon_s$, were given the values used in the computer simulation.

optimum time steps for both the orientational and translational coordinates were approximately the same. We note, however, that this value is not consistent with that for an ellipsoid of revolution of length $3\sigma_0$ and breadth σ_0 with the mass uniformly distributed in it. For this ellipsoid $I_\perp^*$ is just 1/2; however the difference in $I_\perp^*$ is unimportant here because we are only concerned with the structural properties of the phases exhibited by the Gay–Berne mesogen. The symmetry of the potential allows us to decouple the motion about the long axis from the simulation. The equations of motion were integrated using a Verlet algorithm in a method identical to that described by Pollock and Alder [10]. The equations of motion together with the forces and torques obtained from the Gay–Berne potential are listed in the Appendix. In the simulation the scaled density was set equal to 0·30, which is slightly lower than that ($\rho^* = 0{\cdot}32$) employed in the earlier investigation, in an attempt to facilitate the

equilibration of the system. The calculations were performed on an IBM 3090–150 VF where each time step required about 1 s of c.p.u. time for its calculation. In the simulations the scaled time step Δt^*, where t^* is $(\varepsilon_0/m\sigma_0^2)^{1/2}t$ was set equal to 0·005; the scaled times for the equilibration and production stages were typically between 25 and 50.

The first simulation was performed at a high scaled temperature of 3·0 taking a disordered configuration from a previous simulation as the starting point. The equilibrium second rank orientational order parameter, $\bar{P}_2$, was evaluated from the diagonalized Q tensor [11] and found to be approximately 0·09. For such a small number of particles this value indicates that the phase is isotropic; the value is not zero because of the statistical error in evaluating **Q** [12] and the influence of short range angular correlations in a small system. The scaled temperature was then lowered to approximately 2·0, 1·5, 1·0 and 0·5 with the initial configurations for the simulation being taken from the production stage of the preceding temperature. The actual scaled temperatures for the simulations were 3·00, 2·19, 1·49, 1·00 and 0·50. The orientational order parameter was observed to increase with decreasing temperature and to take the values 0·41 ($T^* = 2{\cdot}19$), 0·81 ($T^* = 1{\cdot}49$), 0·91 ($T^* = 1{\cdot}00$) and 0·98 ($T^* = 0{\cdot}50$).

The nature of the phases at these temperatures can be characterized with a range of singlet and pair distribution functions. Thus the orientational order is reflected by the singlet orientational distribution of the molecules with respect to the director. Similarly translational ordering within the smectic phases is contained in the singlet translational distribution function of the molecules along the director. The nature of the molecular organization within a smectic layer could then be determined from the two dimensional radial distribution function together with the bond orientational correlation function. An alternative approach is simply to visualize the arrangement of the particles in a particular configuration taken from the production stage of the simulation. We have adopted the latter approach using an IBM WINGS vector graphics software package. This allows us to manipulate the image in real time and so to examine different features of the molecular organization in the configuration.

3. The mesophases and their identification

Images, photographed from the screen of an IBM 5080 are shown in figure 3 for the simulations at scaled temperatures of approximately 3·00, 2·19, 1·49, 1·00 and 0·50. In the images the molecules are drawn as lines whose length is somewhat shorter than required to be in correct proportion to the size of the simulation box; this enables the molelcular organization to be discerned more easily. In addition the director is also represented in the figures as a thick vertical line through the centre of the box. The orientation of this line with respect to the box was obtained from the Q tensor for the single configuration shown. The length of the director is proportional to the order parameter $\bar{P}_2$ equated with the largest eigenvalue of **Q**, again for the single configuration. Perfect orientational order ($\bar{P}_2 = 1$) corresponds to the director length equal to that of the side of the cube. The configuration at the highest scaled temperature has a low order as is evident from the essentially random arrangement of the molecular orientations (see figure 3 (*a*)). The distribution of the centres of mass is also observably random thus confirming this as the isotropic phase.

At the next lower temperature ($T^* = 2{\cdot}19$, see figure 2 (*b*)) the molecules are clearly orientationally ordered with respect to the director whose length has increased appreciably. The molecular centres of mass are still quite random, in accord with the identification of this as a nematic phase.

The orientational order increases significantly on lowering the scaled temperature to 1·49, as is apparent from the configuration shown in figure 3 (*c*). The molecular organization with respect to the director is more highly ordered as is evidenced by the dramatic growth in the length of the line representing the director. Of greater importance, however, is the clear appearance of a layer structure, orthogonal to the director, albeit with rather weak translational order. We shall return to the nature of this smectic phase presently.

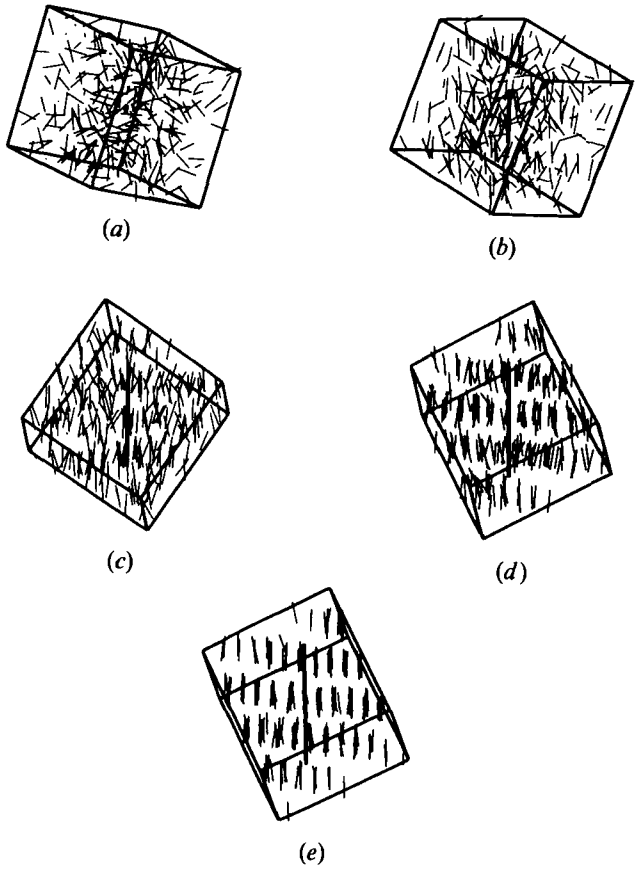

Figure 3. Configurations taken from the production runs of the simulations at scaled temperatures of (*a*) 3·00, (*b*) 2·19, (*c*) 1·49, (*d*) 1·00 and (*e*) 0·50. In these figures the molecules are shown as lines and the director for the configuration is indicated by the thick vertical line whose length is proportional to the second rank orientational order parameter $\bar{P}_2$ for the configuration.

At a still lower temperature ($T^* = 1{\cdot}00$) the orientational order has again grown, as we can see from the molecular distribution with respect to the director; indeed this order is almost complete (see figure 3 (*d*)). Far more obvious is the considerable enhancement of the translational order; the layers are now manifestly apparent. The nature of this smectic phase may simply be a more ordered version of that found at the previous higher temperature or it may be another smectic polymorph. We shall decide this question shortly.

For the sake of completeness a configuration taken from the production run at a scaled temperature of 0·50 is shown in figure 3 (*e*). The essentially perfect order of both

orientational and translational coordinates is very clear. The long range translational ordering occurs in all three dimensions; this can be inferred from the ability to superimpose the molecules within the layers when looking at right angles to the director. The molecular organization within the layers will be considered presently. However the high order of this phase suggests that it is a crystal, a view supported by the vibrational and librational motion of the molecules on lattice sites which contrast with the directly observed diffusional motion of the molecules for the other phases.

We turn now to the molecular organization within the layers and hence an identification of the two smectic phases. To visualize the molecules within a layer we construct a slice with thickness equal to the molecular length σ_e through the cube and orthogonal to the director. This slice is centred on one of the smectic layers, chosen to be near the middle of the simulation box; the layer was located by calculating the singlet translational distribution function along the director for that particular configuration and selecting an appropriate maximum. Those molecules with their centres of mass within the slice are represented as small spheres corresponding to their centres. The image so obtained for the high temperature smectic phase is shown in figure 4(i), (*a*) where the two thick lines at the side of the box indicate the slightly reduced thickness of the slice. The molecular centres of mass are clearly grouped in a layer within the slice but with a reasonable thickness corresponding to weak translational order. For the nematic and isotropic phases the centres of mass are found to be uniformly distributed within the slice. To see the distribution of the molecules within a layer the image was rotated until the director was orthogonal to the IBM 5080 screen. The result is given in figure 4(ii), (*a*) where the centres of mass are found to be distributed randomly within the layer. The high temperature smectic phase can therefore be safely identified as a smectic A [7]. We note that the slice through the simulation box results in some apparent vacancies in the smectic layer. These we attribute both to distortions of the layer and to the penetration of some molecules from one layer into the next.

We have obtained corresponding images for the configuration of the low temperature smectic phase, with the results given in figure 4 (*b*). The thinner layer of the molecular centres shown in figure 4(i), (*b*) corresponds to the higher translational order of the smectic phase. The nature of this smectic phase is revealed in figure 4(ii), (*b*) where the distribution of the centres of mass within the smectic plane is seen to be hexagonal, although this order is not complete. With these limited results and for such a small system it is very difficult to decide on the precise character of the translational order and bond orientational order within the smectic plane. However the tendency of the centres of mass to form a hexagonal arrangement suggests that the mesophase is a smectic B. It is almost impossible to judge whether this should be classified as a hexatic smectic B or a crystal B phase. The image in figure 3 (*d*) suggests that there is some correlation between the positions of particles in different layers but this is not perfect. Whether the correlation extends over many layers as in a crystal B phase [7] or whether it it just short ranged as in a hexatic smectic B phase cannot be discerned without being able to study a larger sample with many more layers.

Again, for the sake of completeness, we show the analogous images in figure 4 (*c*) for the lowest temperature phase ($T^* = 0{\cdot}50$) which we had identified as a crystal. The high translational order, along the orientation of the molecular symmetry axes, is demonstrated by the very narrow distribution of molecular centres within the slice through the simulation box (see figure 4(i), (*c*)). The arrangement of the centres of mass within this plane is given in figure 4(ii), (*c*) and now an essentially long

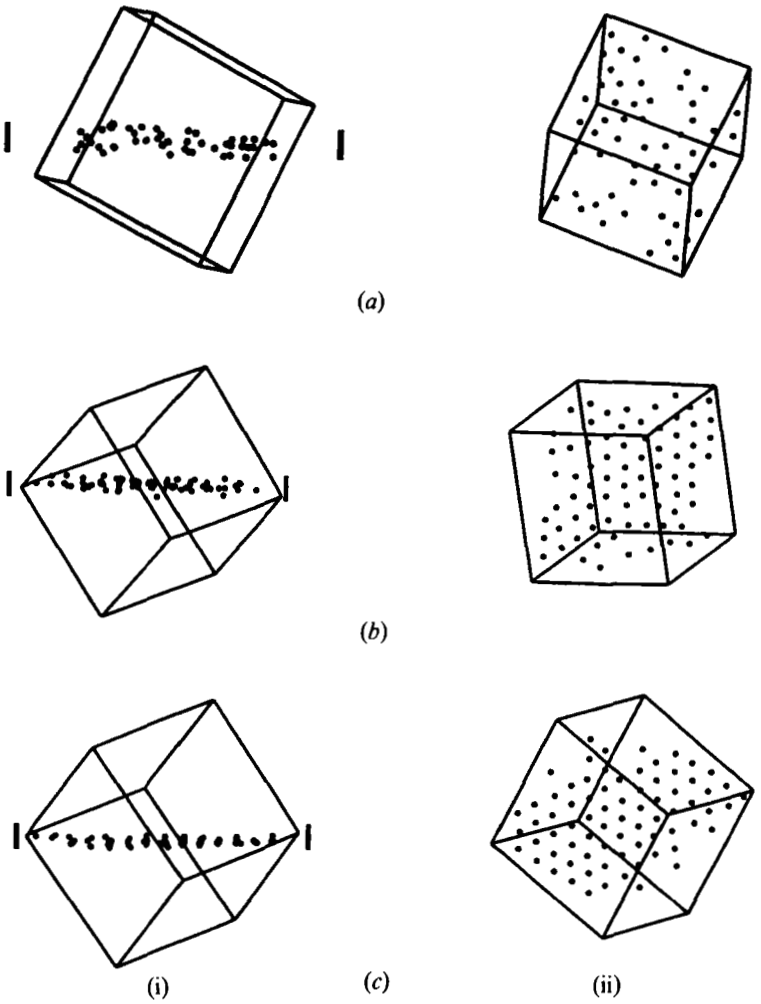

Figure 4. The molecular organization of the centre of masses within a slice of the phase orthogonal to the director, through the centre of a smectic layer and σ_e thick at scaled temperatures of (*a*) 1·49, (*b*) 1·00 and (*c*) 0·50. The images show (i) the distribution across the layer and (ii) that within the layer. The approximate thickness of the slice is indicated by the two lines at the side of the box.

range hexagonal organization is clearly apparent. These images, together with that in figure 3 (*e*), support our identification of this phase as a crystal.

It might have been expected that the simulation box could impose some restrictions on the periodicity of the layer structure characteristic of a smectic phase. Certainly for a system with the director fixed parallel to one side of the box this is clearly the case. Then the density wave of the smectic phase must fit exactly into the box if its layered structured is to be commensurate with its own periodic images. This requires that

$$Nd = L, \tag{8}$$

where d is the layer spacing, L is the length of the cubic simulation box and N is an integer. In our simulations d is of the order of $3\sigma_0$ while the box length is about $9\sigma_0$; thus the ratio L/d is quite small and so its relative deviation from an integer value

could be important. If L/d does deviate from an integer value then the layers in the box will be incommensurate with those in the periodic images and the energy associated with the disclinations so generated could be sufficient to change the layer spacing such that the ratio L/d became integer. However in the simulation the constraint on L/d may not be quite so restrictive as implied by equation (8) because the director need not remain parallel to the edge of the simulation box. For an arbitrary orientation of the director, $\hat{\mathbf{n}}$, the requirement for the continuity of the smectic layers in the simulation box with those of its periodic images requires

$$N_\alpha \hat{n}_\alpha d = L, \tag{9}$$

where N_α is an integer and α denotes x, y and z. Since $\hat{\mathbf{n}}$ is a unit vector we see that the constraint placed on d takes the form

$$d = L/(N_x^2 + N_y^2 + N_z^2)^{1/2}, \tag{10}$$

which is somewhat easier to satisfy than equation (8). For example, there the ratio L/d must be say either 3 or 4 whereas a range of values of L/d between 3 and 4 can be obtained from the constraint imposed by equation (10). We expect, therefore, that the director for the smectic phases will adopt an orientation within the simulation box such that equation (10) is, to a good approximation, satisfied. This certainly seems to be the case for the system which we have studied. We should also note that equation (10) is identical to that for the spacing between adjacent layers with Miller indices N_x, N_y, N_y for a cubic lattice with periodicity L. For such a system the layers within the unit cell of the lattice (i.e. the simulation box) are clearly commensurate with those in all other unit cells (i.e. the periodic images).

Analogous conditions obtain within the layers of the more ordered smectic phases and in the crystal. However there are no ways in which the system can satisfy these once the director orientation has been determined by the periodicity of the smectic layers. Fortunately the periodicity, a, within a layer is relatively small so that the ratio $(L/a)^2$ will be large, which means that the deviations from an integer value will be proportionally smaller. None the less for such high ordered systems it would be of particular interest to perform the simulation at constant pressure rather than constant volume. This would allow the box shape to be changed thus revealing the true structure unperturbed by the influence of the periodic boundary conditions [13].

4. Conclusion

A system of particles interacting via the Gay–Berne potential with a particular choice of parameters ($\sigma_e/\sigma_s = 3, \varepsilon_e/\varepsilon_s = 1/5, \nu = 2, \mu = 1$) has been investigated by the molecular dynamics simulation technique. The system is found to exhibit a series of phases as the temperature is lowered. These phases have been identified by using computer graphics to visualize configurations taken from the production stage of the simulation. It would seem that the system possesses an isotropic, a nematic, a smectic A, a smectic B (hexatic or crystal) and a crystal phase. This rich polymorphism of the Gay–Berne model mesogen makes it an ideal system with which to enhance our understanding of the static and dynamic behaviour of real liquid crystals.

We are grateful to the Science and Engineering Research Council for the award of a research studentship to Mr. R. A. Stephens and for a grant towards the cost of the IBM graphics system.

Appendix

Here, for the benefit of those readers unfamiliar with the molecular dynamics simulation technique, we provide a brief description of the methodology used in this paper. We also give the somewhat cumbersome expressions for the forces and torques for the Gay–Berne potential since these will be of value for those wishing to use this valuable model for liquid crystals in other simulation studies.

The equations of motion for a particle can be separated into those concerned with translation and those dealing with rotation. The equation for the motion of the centre of mass is

$$m\ddot{\mathbf{r}} = \mathbf{F}; \tag{A 1}$$

here m is the total mass of the particle, $\mathbf{F}$ is the total force acting on it and $\ddot{\mathbf{r}}$ is the acceleration of the particle caused by the force. For a molecule composed of several sites i the total mass is simply

$$m = \sum_i m_i, \tag{A 2}$$

where m_i is the mass associated with site i. The total force is then just the sum of the forces, $\mathbf{F}_i$, acting on each site

$$\mathbf{F} = \sum_i \mathbf{F}_i. \tag{A 3}$$

The force on site i is the sum of those forces resulting from its interaction with all other particles in the simulation box and its periodic images. For an interaction between two sites via the potential U the force on site i at $(x_i y_i z_i)$ is

$$\mathbf{F}_i = -\begin{pmatrix} (\partial U/\partial x_i) \\ (\partial U/\partial y_i) \\ (\partial U/\partial z_i) \end{pmatrix}. \tag{A 4}$$

The rotational analogues of these equations are

$$\mathbf{I}\dot{\boldsymbol{\omega}} = \boldsymbol{\tau}, \tag{A 5}$$

where $\mathbf{I}$ is the moment of inertia tensor, $\boldsymbol{\tau}$ is the torque acting on the particle and $\dot{\boldsymbol{\omega}}$ is the resultant angular acceleration. For a particle containing several sites

$$\mathbf{I} = \sum_i m_i(\mathbf{r}_i - \mathbf{r})(\mathbf{r}_i - \mathbf{r}), \tag{A 6}$$

where $\mathbf{r}$ denotes the centre-of-mass coordinates. The torque $\boldsymbol{\tau}$ acting on the particle is defined in terms of the forces acting on each site by

$$\boldsymbol{\tau} = \sum_i (\mathbf{r}_i - \mathbf{r}) \times \mathbf{F}_i. \tag{A 7}$$

The Gay–Berne potential is, however, a single site potential, indeed this is one of its virtues. The particle does, of course, experience a torque because of the angular dependence of the potential. This torque is equivalent to a force acting on a point separated by a unit distance from the centre-of-mass and acting in a direction orthogonal to the molecular symmetry axis. This equivalent force can be defined in terms of the derivative of the potential with respect to the coordinates of this point where the centre-of-mass is taken as the origin. These coordinates are just the

components of the unit vector $\hat{\mathbf{u}}_1$ describing the molecular orientation and so the equivalent force is

$$\mathbf{E} = -\begin{pmatrix} (\partial U/\partial \hat{u}_{1x}) \\ (\partial U/\partial \hat{u}_{1y}) \\ (\partial U/\partial \hat{u}_{1z}) \end{pmatrix} \tag{A 8}$$

and the torque is then

$$\boldsymbol{\tau} = \hat{\mathbf{u}}_1 \times \mathbf{E}. \tag{A 9}$$

The equations of motion for the centre-of-mass coordinates are solved using the Verlet algorithm [14]

$$\mathbf{r}(t + \delta t) = 2\mathbf{r}(t) - \mathbf{r}(t - \delta t) + \ddot{\mathbf{r}}(t)\delta t^2. \tag{A 10}$$

The equations of motion for the molecular orientation can, in principle, be solved for the time evolution of the unit vector $\hat{\mathbf{u}}$ in the same way,

$$\mathbf{u}(t + \delta t) = 2\hat{\mathbf{u}}(t) - \hat{\mathbf{u}}(t - \delta t) + \ddot{\hat{\mathbf{u}}}(t)\delta t^2, \tag{A 11}$$

where the angular acceleration $\ddot{\hat{\mathbf{u}}}(t)$ is

$$\ddot{\hat{\mathbf{u}}}(t) = \mathbf{E}/\mathbf{I}. \tag{A 12}$$

For sufficiently small time steps the vector $\mathbf{u}$ at time $t + \delta t$ would be a unit vector but, in general, there is no constraint on $\mathbf{u}(t + \delta t)$ to have unit length and so the hat has been removed from this in equation (A 11). To prevent $\mathbf{u}(t + \delta t)$ from deviating from its desired unit length a corrective force is, in effect, applied parallel to the molecular symmetry axis, at time t. The magnitude, λ, of this force

$$\mathbf{f}(t) = \lambda \hat{\mathbf{u}}(t) \tag{A 13}$$

is chosen to retain $\hat{\mathbf{u}}(t + \delta t)$ as a unit vector. It has no other effect on the dynamics of the system. The value of $\lambda(t)$ necessary to achieve this is found in the following way. The force applied is such that at the end of the time step $\mathbf{u}(t + \delta t)$ is a unit vector, that is

$$\hat{\mathbf{u}}'(t + \delta t) = \mathbf{u}(t + \delta t) + \hat{\mathbf{u}}(t)(\lambda/2\tilde{m})\delta t^2, \tag{A 14}$$

where $\tilde{m}$ is an arbitrary mass on which $\mathbf{f}(t)$ acts. However the value of $\tilde{m}$ can be subsumed into λ by writing equation (A 14) as

$$\hat{\mathbf{u}}'(t + \delta t) = \mathbf{u}(t + \delta t) + \hat{\mathbf{u}}(t)\lambda'. \tag{A 15}$$

Now taking the scalar product of each side of this equation with itself gives a quadratic for λ' whose solution is

$$\lambda' = -\hat{\mathbf{u}}(t) \cdot \mathbf{u}(t + \delta t) \pm \{[\hat{\mathbf{u}}(t) \cdot \mathbf{u}(t + \delta t)]^2 - [\mathbf{u}(t + \delta t) \cdot \mathbf{u}(t + \delta t)] + 1\}^{1/2}. \tag{A 16}$$

The positive sign is taken since this will always give the smallest value for λ' and so ensure that the correction terms are minimized. These terms $\hat{\mathbf{u}}(t)\lambda'$ are then added to the vector $\mathbf{u}(t + \delta t)$ which restores the molecular orientation at time $t + \delta t$ to being a unit vector.

We turn now to the gradients of the Gay–Berne potential needed in the integrated equations of motion. To simplify the notation equation (1) for the potential is written in terms of the scaled variable

$$R = [r - \sigma(\hat{\mathbf{u}}_1, \hat{\mathbf{u}}_2, \hat{\mathbf{r}}) + \sigma_0]/\sigma_0. \tag{A 17}$$

The function, depending on the relative orientation of the molecules and the intermolecular vector, which enters the expressions for both the well depth and the distance of closest approach is written as

$$g(X) = 1 - \frac{X}{2}\left\{\frac{(\hat{\mathbf{r}}\cdot\hat{\mathbf{u}}_1 + \hat{\mathbf{r}}\cdot\hat{\mathbf{u}}_2)^2}{1 + X(\hat{\mathbf{u}}_1\cdot\hat{\mathbf{u}}_2)} + \frac{(\hat{\mathbf{r}}\cdot\hat{\mathbf{u}}_1 - \hat{\mathbf{r}}\cdot\hat{\mathbf{u}}_2)^2}{1 - X(\hat{\mathbf{u}}_1\cdot\hat{\mathbf{u}}_2)}\right\}. \tag{A 18}$$

Here X denotes either the shape anisotropy parameter χ or the well-depth anisotropy parameter χ'; that is

$$g(\chi)^{-1/2} = \sigma(\hat{\mathbf{u}}_1, \hat{\mathbf{u}}_2, \hat{\mathbf{r}})/\sigma_0 \tag{A 19}$$

and

$$g(\chi') = \varepsilon'(\hat{\mathbf{u}}_1, \hat{\mathbf{u}}_2, \hat{\mathbf{r}}). \tag{A 20}$$

As the translational coordinate of one molecule is changed so the components of the intermolecular vector are also altered. To make this dependence of $\sigma(\hat{\mathbf{u}}_1, \hat{\mathbf{u}}_2, \hat{\mathbf{r}})$ and $\varepsilon'(\hat{\mathbf{u}}_1, \hat{\mathbf{u}}_2, \hat{\mathbf{r}})$ on the intermolecular separation explicit we write $g(X)$ in terms of the intermolecular vector $\mathbf{r}$ and the separation r,

$$g(X) = 1 - \frac{X}{2r^2}\left\{\frac{(\mathbf{r}\cdot\hat{\mathbf{u}}_1 + \mathbf{r}\cdot\hat{\mathbf{u}}_2)^2}{1 + X(\hat{\mathbf{u}}_1\cdot\hat{\mathbf{u}}_2)} + \frac{(\mathbf{r}\cdot\hat{\mathbf{u}}_1 - \mathbf{r}\cdot\hat{\mathbf{u}}_2)^2}{1 - X(\hat{\mathbf{u}}_1\cdot\hat{\mathbf{u}}_2)}\right\}. \tag{A 21}$$

Using this notation the gradient of the Gay–Berne potential with respect to, say, the x coordinate of one particle is

$$\frac{\partial U}{\partial x} = \varepsilon_0\left\{\varepsilon^{\nu}(\hat{\mathbf{u}}_1, \hat{\mathbf{u}}_2)g^{\mu}(\chi')[6R^{-7} - 12R^{-13}](\partial R/\partial x) + (R^{-12} - R^{-6})\mu g^{\mu-1}(\chi')\frac{\partial g(\chi')}{\partial x}\right\}, \tag{A 22}$$

where

$$\partial R/\partial x = \partial r/\partial x + \frac{\sigma_0}{2}g^{-3/2}(\chi)\frac{\partial g(\chi)}{\partial x}, \tag{A 23}$$

$$\partial r/\partial x = x/r, \tag{A 24}$$

$$\frac{\partial g(X)}{\partial x} = -\frac{X}{r^2}\left[\frac{[\mathbf{r}\cdot\hat{\mathbf{u}}_1 + \mathbf{r}\cdot\hat{\mathbf{u}}_2]}{1 + X[\hat{\mathbf{u}}_1\cdot\hat{\mathbf{u}}_2]}\left\{\frac{\partial(\mathbf{r}\cdot\hat{\mathbf{u}}_1)}{\partial x} + \frac{\partial(\mathbf{r}\cdot\hat{\mathbf{u}}_2)}{\partial x}\right\} + \frac{[\mathbf{r}\cdot\hat{\mathbf{u}}_1 - \mathbf{r}\cdot\hat{\mathbf{u}}_2]}{1 - X[\hat{\mathbf{u}}_1\cdot\hat{\mathbf{u}}_2]}\left\{\frac{\partial(\mathbf{r}\cdot\hat{\mathbf{u}}_1)}{\partial x} - \frac{\partial(\mathbf{r}\cdot\hat{\mathbf{u}}_2)}{\partial x}\right\}\right] + \frac{xX}{r^4}\left[\frac{(\mathbf{r}\cdot\hat{\mathbf{u}}_1 + \mathbf{r}\cdot\hat{\mathbf{u}}_2)^2}{1 + X[\hat{\mathbf{u}}_1\cdot\hat{\mathbf{u}}_2]} + \frac{(\mathbf{r}\cdot\hat{\mathbf{u}}_1 - \mathbf{r}\cdot\hat{\mathbf{u}}_2)^2}{1 - X[\hat{\mathbf{u}}_1\cdot\hat{\mathbf{u}}_2]}\right], \tag{A 25}$$

$$\frac{\partial(\mathbf{r}\cdot\hat{\mathbf{u}}_1)}{\partial x} = \hat{u}_{1x} \quad \text{and} \quad \frac{\partial(\mathbf{r}\cdot\hat{\mathbf{u}}_2)}{\partial x} = \hat{u}_{2x}. \tag{A 26}$$

There are analogous expressions for the y and z derivatives which then give the force $\mathbf{F}$ acting on a particle (see equation (A 4)).

The torque is obtained in a similar manner; we give the gradient of the potential with respect to the x component of the unit vector $\hat{\mathbf{u}}_1$. This is

$$\frac{\partial U}{\partial \hat{u}_{1x}} = (R^{-12} - R^{-6}) \frac{\partial \varepsilon(\hat{\mathbf{u}}_1, \hat{\mathbf{u}}_2, \hat{\mathbf{r}})}{\partial \hat{u}_{1x}} + \varepsilon(\hat{\mathbf{u}}_1, \hat{\mathbf{u}}_2, \hat{\mathbf{r}})(6R^{-7} - 12R^{-13}) \frac{\partial R}{\partial \hat{u}_{1x}}, \quad \text{(A 27)}$$

where

$$\frac{\partial \varepsilon(\hat{\mathbf{u}}_1, \hat{\mathbf{u}}_2, \hat{\mathbf{r}})}{\partial \hat{u}_{1x}} = \varepsilon_0 \varepsilon^{\nu}(\hat{\mathbf{u}}_1, \hat{\mathbf{u}}_2) \mu g^{\mu-1}(\chi') \frac{\partial g(\chi')}{\partial \hat{u}_{1x}} + \varepsilon_0 g^{\mu}(\chi') \nu \varepsilon^{\nu-1}(\hat{\mathbf{u}}_1, \hat{\mathbf{u}}_2) \frac{\partial \varepsilon(\hat{\mathbf{u}}_1, \hat{\mathbf{u}}_2)}{\partial \hat{u}_{1x}}. \quad \text{(A 28)}$$

The derivatives occurring in these equations are given by

$$\frac{\partial \varepsilon(\hat{\mathbf{u}}_1, \hat{\mathbf{u}}_2)}{\partial \hat{u}_{1x}} = \chi^2 \varepsilon^3(\hat{\mathbf{u}}_1, \hat{\mathbf{u}}_2) \hat{u}_{2x}, \quad \text{(A 29)}$$

$$\frac{\partial R}{\partial \hat{u}_{1x}} = -(1/\sigma_0) \frac{\partial \sigma(\hat{\mathbf{u}}_1, \hat{\mathbf{u}}_2, \hat{\mathbf{r}})}{\partial \hat{u}_{1x}} = (1/2) \left\{ \frac{\sigma(\hat{\mathbf{u}}_1, \hat{\mathbf{u}}_2, \hat{\mathbf{r}})}{\sigma_0} \right\}^3 \frac{\partial g(\chi)}{\partial \hat{u}_{1x}}, \quad \text{(A 30)}$$

where

$$\frac{\partial g(X)}{\partial \hat{u}_{1x}} = -\frac{X}{2} \left[\hat{r}_x \left\{ \frac{2(\hat{\mathbf{r}} \cdot \hat{\mathbf{u}}_1 + \hat{\mathbf{r}} \cdot \hat{\mathbf{u}}_2)}{1 + X[\hat{\mathbf{u}}_1 \cdot \hat{\mathbf{u}}_2]} + \frac{2(\hat{\mathbf{r}} \cdot \hat{\mathbf{u}}_1 - \hat{\mathbf{r}} \cdot \hat{\mathbf{u}}_2)}{1 - X[\hat{\mathbf{u}}_1 \cdot \hat{\mathbf{u}}_2]} \right\} + X \hat{u}_{2x} \left\{ \frac{(\hat{\mathbf{r}} \cdot \hat{\mathbf{u}}_1 - \hat{\mathbf{r}} \cdot \hat{\mathbf{u}}_2)^2}{1 - X[\hat{\mathbf{u}}_1 \cdot \mathbf{u}_2]^2} + \frac{(\hat{\mathbf{r}} \cdot \hat{\mathbf{u}}_1 + \hat{\mathbf{r}} \cdot \hat{\mathbf{u}}_2)^2}{1 + X[\hat{\mathbf{u}}_1 \cdot \hat{\mathbf{u}}_2]^2} \right\} \right]. \quad \text{(A 31)}$$

References

[1] DEMUS, D., 1989, *Liq. Crystals*, **5**, 75.

[2] LEBWOHL, P. A., and LASHER, G., 1972, *Phys. Rev.* A, **6**, 426; 1973, *Ibid.*, **7**, 2222.

[3] BERNE, B. J., and PECHUKAS, P., 1972, *J. chem. Phys.*, **56**, 4213. KUSHICK, J., and BERNE, B. J., 1976, *J. chem. Phys.*, **64**, 1362.

[4] STONE, A. J., 1979, *The Molecular Physics of Liquid Crystals*, edited by G. R. Luckhurst and G. W. Gray (Academic Press), chap. 2.

[5] GAY, J. G., and BERNE, B. J., 1981, *J. chem. Phys.*, **74**, 3316. N.b. the notation introduced by Gay and Berne for the potential differs slightly from that which we use here.

[6] ADAMS, D. J., LUCKHURST, G. R., and PHIPPEN, R. W., 1987, *Molec. Phys.*, **61**, 1575. This paper contains several typographical errors: in the simulation $\varepsilon_e/\varepsilon_s$ was set equal to 1/5 (and not 5); the parameters in the potential had been obtained [5] for four Lennard-Jones centres separated by $2\sigma_0$ (and not $3\sigma_0$) and the temperatures labelling the second rank pair correlation functions in figure 1 should be reversed.

[7] See, for example, LEADBETTER, A. J., 1987, *Thermotropic Liquid Crystals*, edited by G. W. Gray (Wiley).

[8] FRENKEL, D., 1988, *J. phys. Chem.*, **92**, 3280.

[9] FRENKEL, D., 1989, *Liq. Crystals*, **5**, 929.

[10] POLLOCK, E. L., and ALDER, B. J., 1980, *Physica* A, **102**, 1.

[11] VIEILLARD-BARON, J., 1974, *Molec. Phys.*, **28**, 809.

[12] EPPENGA, R., and FRENKEL, D., 1984, *Molec. Phys.*, **52**, 1303.

[13] PARRINELLO, M., and RAHMAN, A., 1981, *J. appl. Phys.*, **52**, 7182.

[14] VERLET, L., 1967, *Phys. Rev.*, **159**, 98.